
University of Alaska

Coastal Marine Institute



Observations of hydrography and currents in central Cook Inlet, Alaska during diurnal and semidiurnal tidal cycles

Stephen R. Okkonen, Principal Investigator
Institute of Marine Science, University of Alaska Fairbanks

Final Report

October 2005

OCS Study MMS 2004-058

OCS STUDY MMS 2004-058

Final Report

**Observations of hydrography and currents in central Cook
Inlet, Alaska during diurnal and semidiurnal tidal cycles**

by

Stephen R. Okkonen
Institute of Marine Science
University of Alaska Fairbanks

SEPTEMBER 2005

Contact information

e-mail: carter@sfos.uaf.edu

phone: 907.474.1811

fax: 907.474.1188

postal: Coastal Marine Institute
School of Fisheries and Ocean Sciences
University of Alaska Fairbanks
Fairbanks, AK 99775-7220

Table of Contents

Table of Figures	ii
Abstract	1
Background and Relevance to Framework Issues.....	1
Methods.....	2
Results	3
<i>Mean property fields</i>	3
<i>Semidiurnal variability</i>	4
<i>Diurnal variability</i>	5
Discussion	6
References	8

Table of Figures

Figure 1. Bathymetric map and place names of Cook Inlet, Alaska. The location of the hydrographic section is shown as a red line.	9
Figure 2. MODIS true color image of Cook Inlet acquired 2 September 2002.	10
Figure 3. (Top) Mean surface currents vectors across section. Northward flow is up, southward flow is down. (Bottom) Mean salinity across section. Contour interval is 1.0 psu.	11
Figure 4. (Top) Mean surface currents vectors. Northward flow is up, southward flow is down. (Bottom) Mean temperature across section. Contour interval is 1.0° C.	12
Figure 5. (Top) Mean surface currents vectors. Northward flow is up, southward flow is down. (Bottom) Mean baroclinic geostrophic velocity across section. Positive speeds are northward. Contour interval 0.5 kt.	13
Figure 6. (Top) Mean surface currents vectors. Northward flow is up, southward flow is down. (Bottom) Mean transmissivity across section. Contour interval is 10%.	14
Figure 7. (Top) Semidiurnal (M2) tidal ellipses. Northward flow is up, southward flow is down. (Middle) Phase of semidiurnal tidal currents. Phase is relative to 00 hours, 9 August 2003 local time. (Bottom) Bottom depth profile along section.	15
Figure 8. a) Amplitude of semidiurnal salinity signal. Contour interval is 0.2 psu. b) Phase of semidiurnal salinity signal relative to 00 hours, 9 August 2003 local time. Contour interval is 1.0 hours.	16
Figure 9. a) Amplitude of semidiurnal temperature signal. Contour interval is 0.1°C. b) Phase of semidiurnal salinity signal relative to 00 hours, 9 August 2003 local time. Contour interval is 1.0 hours.	17
Figure 10. a) Amplitude of semidiurnal transmissivity signal. Contour interval 5%. b) Phase of semidiurnal salinity signal relative to 00 hours, 9 August 2003 local time. Contour interval is 1.0 hours.	18
Figure 11. (Top) Diurnal (K1) tidal ellipses. Northward flow is up, southward flow is down. (Bottom) Phase of semidiurnal tidal currents. Phase is relative to 00 hours, 9 August 2003 local time. (Bottom) Bottom depth profile along section.	19
Figure 12. a) Amplitude of diurnal salinity signal. Contour interval is 0.2 psu. b) Phase of diurnal salinity signal relative to 00 hours, 9 August 2003 local time. Contour interval is 1 hour.	20
Figure 13. a) Amplitude of diurnal temperature signal. Contour interval is 0.1° C. b) Phase of diurnal salinity signal relative to 00 hours, 9 August 2003 local time. Contour interval is 1 hour.	21
Figure 14. a) Amplitude of diurnal transmissivity signal. Contour interval 5%. b) Phase of diurnal salinity signal relative to 00 hours, 9 August 2003 local time. Contour interval is 1 hour.	22
Figure 15. (Top) Time-longitude plot of cross-channel surface current divergence ($\partial u/\partial x$). Contour interval is $1 \times 10^{-4} \text{ s}^{-1}$. Convergence ($\partial u/\partial x < 0$) is shaded. Divergence ($\partial u/\partial x > 0$) is not shaded. Surface current vectors are shown. Thick dotted lines denote slack water (northward and southward current components are zero). Occurrences of (H)igh and (L)ow tides indicated on right side of plot. (Bottom) Bottom depth profile along section.	23

Figure 16. (Top) Time-longitude plot of along-channel surface current shear ($\partial v/\partial x$). Contour interval is $1 \times 10^{-4} \text{ s}^{-1}$. Negative shears ($\partial v/\partial x < 0$) are shaded. Surface current vectors are shown. Thick dotted lines denote slack water (northward and southward current components are zero). Occurrences of (H)igh and (L)ow tides indicated on right side of plot. (Bottom) Bottom depth profile along section. 24

Figure 17. (Top) Time-longitude plot of surface layer salinity (0–1 m). Contour interval is 0.5 psu. Surface current vectors are shown. Thick dotted lines denote slack water (northward and southward current components are zero). Occurrences of (H)igh and (L)ow tides indicated on right side of plot. White oblique lines indicate vessel position and time. (Bottom) Bottom depth profile along section..... 25

Figure 18. Map of bathymetric gradients in Cook Inlet, Alaska..... 26

Figure 19. Synthetic aperture radar image (8 February 2000) of central Cook Inlet, Alaska..... 27

Observations of hydrography and currents in central Cook Inlet, Alaska during diurnal and semidiurnal tidal cycles

Stephen R. Okkonen
Institute of Marine Science
University of Alaska Fairbanks

Abstract

Surface-to-bottom measurements of temperature, salinity, and transmissivity, as well as measurements of surface currents (vessel drift speeds) were acquired along an east-west section in central Cook Inlet, Alaska during a 26-hour period on 9–10 August 2003. These measurements are used to describe the evolution of frontal features (tide rips) and physical properties along this section during semidiurnal and diurnal tidal cycles. The observation that the amplitude of surface currents is a function of water depth is used to show that strong frontal features occur in association with steep bathymetry. The positions and strengths of these fronts vary with the semidiurnal tide. The presence of freshwater gradients alters the phase and duration of tidal currents across the section. Where mean density-driven flow is northward (along the eastern shore and near Kalgin Island), the onset of northward tidal flow (flood tide) occurs earlier and has longer duration than the onset and duration of northward tidal flow where mean density-driven flow is southward (in the shipping channel). Conversely, where mean density-driven flow is southward (in the shipping channel), the onset of southward tidal flow (ebb tide) occurs earlier and has longer duration than the onset and duration of southward tidal flow along the eastern shore and near Kalgin Island.

Background and Relevance to Framework Issues

Cook Inlet, a large (~350 km long) tidal estuary in southcentral Alaska (Figure 1), is oriented roughly south-southwest to north-northeast. Northern inlet waters are relatively fresh (<20 psu) and turbid owing to sediment-laden discharges from the Matanuska, Susitna and Knik rivers. The southern inlet opens to Shelikof Strait and the shelf region of the northern Gulf of Alaska. The relatively clear oceanic waters occupying the southern inlet intrude northward along the eastern side of the central inlet (Figure 2). The north-south salinity gradient is strongest in late summer/early fall when river discharges and glacial outflows are high. Semidiurnal tidal currents dominate circulation variability in Cook Inlet and establish strong frontal convergence zones known locally as the West Rip, Middle Rip, and East Rip. These strong rips serve as migratory pathways for salmon returning to their natal streams and forage sites for sea birds. During the 1987 T/V Glacier Bay oil spill, these convergent rips collected spilled oil.

This study investigates the semidiurnal and diurnal variability of the hydrographic structure and currents in central Cook Inlet during conditions associated with the neap-to-spring progression of the fortnightly tidal cycle and with large freshwater inputs. However, the operative physical forces and their periods of variability are known, so that the results can be extended to infer conditions at other locations in Cook Inlet and at other times during the fortnightly tidal cycle and seasonal freshwater cycle. The results from this project (1) improve the understanding of local hydrography, surface currents, and dynamical processes, (2) provide observations for the development and validation of numerical circulation models, and (3) provide information that may be potentially useful for spill response planning and training.

Methods

A Sea-Bird Electronics, Inc. SBE 19plus SEACAT Profiler CTD (conductivity-temperature-depth) and a WET Labs C-STAR transmissometer were used to acquire 126 surface-to-bottom measurements of temperature, salinity, and light transmissivity during nine crossings of an east-west transect near Kalgin Island and Kenai/Soldotna in central Cook Inlet, Alaska (see Figure 1). GPS measurements of vessel drift speed and direction were also recorded at each CTD cast location. These measurements were acquired during a 26.5 hour period beginning 12:35 hours (local time) on 9 August 2003. The sampling period was chosen to occur during a period of calm seas and light winds so as to reflect oceanographic conditions without the complicating effects of wind and waves influencing surface currents or mixing of the water column. Seas were calm (less than 2 ft.) and mean winds were light (6.3 kts, 3.2 m s^{-1}) during this period and, as a consequence, wind and wave effects were considered to be negligible and vessel drift velocities were assumed to represent surface current velocities. High tides at the Kenai River entrance (5 km north of the eastern terminus of the transect) during the sampling period were approximately 18.9 ft (5.76 m) at 15:45 (9 August 2003) and 21.3 ft (6.49 m) at 03:13 (10 August 2003) local time. Low tides at the Kenai River entrance were approximately 5.0 ft (1.52 m) at 21:30 (9 August 2003) and -1.7 ft (-0.52 m) at 10:23 (10 August 2003).

Station spacing between successive CTD casts was nominally 1.82 km (1 n mi.) near the coasts and 2.73 km (1.5 n mi.) along the middle portion of the transect. Cast locations were acquired from a vessel-mounted GPS unit. Vessel drift velocities (speeds and headings) were calculated automatically by the GPS unit from successive GPS fixes. The CTD was lowered at approximately 30 m min^{-1} and individual measurements of temperature, salinity, transmissivity, and pressure were acquired at a rate of four per second. Temperature, salinity, and transmissivity data from each downcast were averaged in 1 m (1 decibar) bins centered on integer depths.

Sampling along each crossing of the transect took roughly 3 hours. As a consequence, a temporal offset is associated with each CTD station location. In order to depict instantaneous conditions across the transect, a least squares procedure was used to compute interpolated values of temperature, salinity, and transmissivity at 15-minute intervals for each integer depth at each CTD station location. The underlying assumption for the interpolation was that conditions at each location x and depth z varied according to the sinusoidal function

$$P(t) = A_1 \cdot \cos(2\pi \cdot t / 12.42) + A_2 \cdot \sin(2\pi \cdot t / 12.42) + A_3 \cdot \cos(2\pi \cdot t / 23.93) + A_4 \cdot \sin(2\pi \cdot t / 23.93) + A_5 \cdot t + A_6 \quad (\text{Equation 1})$$

in which P is the property of interest (temperature, salinity, transmissivity, or velocity), $A_1 \dots A_6$ are least squares coefficients, and t is the time in hours. The function includes the M2 semidiurnal (12.42 hr) tidal constituent, the K1 diurnal (23.93 hr) tidal constituent, a linear trend, and offset.

The amplitude and phase of the M2 semidiurnal variation were computed according to

$$\text{Amplitude}_{M2} = (A_1^2 + A_2^2)^{1/2} \quad (\text{Equation 2})$$

$$\text{Phase}_{M2} = \tan^{-1}(A_2/A_1), \quad (\text{Equation 3})$$

respectively. Similarly, the amplitude and phase of the K1 diurnal variation were computed according to

$$\text{Amplitude}_{K1} = (A_3 \cdot A_3 + A_4 \cdot A_4)^{1/2} \quad (\text{Equation 4})$$

$$\text{Phase}_{K1} = \tan^{-1} (A_4/A_3). \quad (\text{Equation 5})$$

Daily-mean property fields were computed by averaging the ninety-six 15-minute property fields computed according to equation 1 for the 24-hour period beginning 1400 hrs, 9 August 2003.

The terms flood tide and ebb tide are used in reference to tidal currents that flow up-inlet and down-inlet, respectively, as opposed to tidal heights.

Results

Mean property fields

The daily-mean salinity field illustrates representative structures and locations of the principal salinity fronts in central Cook Inlet (Figure 3). Two freshwater (<25 psu) plumes intersect the transect. The plume along the eastern side of the inlet (<23 psu) derives from the Kenai and Kasilof Rivers (east plume). The surface plume in the shipping channel (<25 psu) is the extension of freshwater originating in the northern inlet that has passed through the constriction between the West Foreland and East Foreland (Forelands plume). The shipping channel refers to the relatively deep channel that intersects the section roughly between 151.73°W and 151.55°W. The strong salinity gradients at the flanks of the Forelands plume define two fronts, the surface expressions of which are locally known as the West Rip and Middle Rip. The Middle Rip front is the most vertically extensive of these fronts. The base of the Middle Rip front intersects the bottom at a depth of approximately 50 m. The most saline waters (>27 psu) are found at the bottom of the shipping channel and in the shallows adjacent to Kalgin Island. The higher salinity values occurring in the shipping channel reflect the northward intrusion of denser water with a more oceanic character. Mean surface currents, shown in stick plot format above the mean salinity field, indicate that mean flow associated with the core of the Forelands plume is southward and northward elsewhere. The changes between northward and southward flows occur where the depth-averaged zonal salinity gradient changes sign (near 151.72°W and 151.59°W).

The structure of the mean temperature field (Figure 4) is qualitatively similar to the structure of the mean salinity field in that the locations of the thermal fronts roughly correspond to the locations of the salinity fronts, although the temperatures and salinities are negatively correlated. Temperatures and salinities are negatively correlated during the summer months, whereas they are positively correlated during the winter months. While the warmest temperatures (>15°C) occur along the shallow eastern side of the inlet, temperatures associated with the Forelands plume are also slightly warmer (>14°C) than adjacent waters. The coolest temperatures (<13.4°C) are found at the bottom of the shipping channel.

The mean salinity and temperature fields were used to compute a mean density field, from which were computed the baroclinic geostrophic currents normal to the section line (Figure 5). The contour plot indicates that density-driven currents are generally northward across the section except within the shipping channel where mean currents are southward. The stick plot of mean surface currents, independently derived from vessel drift velocities, shows directions similar in orientation to the baroclinic currents, but it shows somewhat different magnitudes. The mean salinity field (see Figure 3) and geostrophy provide the context for understanding the mean current field. Because the temperature gradients are relatively weak (see Figure 4), density

gradients are more greatly influenced by the relatively strong salinity gradients (see Figure 3). According to the geostrophic approximation, northward baroclinic geostrophic currents will be associated with an eastward decrease in density (fresher and warmer), whereas southward geostrophic currents will be associated with an eastward increase in density (saltier and cooler). This description of mean surface currents differs somewhat from those provided by Burbank (1977) and Whitney (1994), in which they both show southward flow everywhere at this latitude except very near the eastern side of the inlet.

The structure of mean transmissivity field (Figure 6) differs somewhat from the general structure of the mean salinity and temperature fields. Transmissivity is functionally related to the suspended sediment concentration, although water samples were not taken to quantify this relationship. Low (high) transmissivity is associated with a high (low) suspended sediment concentration. Overall, the suspended sediment concentration increases with depth. The clearest waters occur above the eastern flank of the shipping channel in association with higher salinity, more oceanic waters and on the seaward flank of the East plume (compare with Figure 3). The highest suspended sediment concentrations generally occur where the mean current speeds are high, that is, above the western flank of the shipping channel and midway between the shipping channel and the eastern side of the inlet.

Semidiurnal variability

Mean semidiurnal surface current tidal ellipses and phases along the transect are shown in Figure 7. The largest amplitude semidiurnal currents (>4 kts) occur in the deep water of the shipping channel and are more or less aligned with the NNE-SSW axis of the channel. As the bottom shoals toward the eastern side of the inlet, the semidiurnal currents generally weaken except for a slight intensification at the two easternmost stations. Adding the semidiurnal tidal currents to their corresponding mean currents (see Figure 3) suggests that the strongest net currents during the flood tide will be observed near 151.63°W, whereas the strongest currents during the ebb tide will be observed between 151.67°W and 151.7°W. The meridional current components at the three stations nearest Kalgin Island are about 2 knots. Interestingly, the zonal current components at 151.8°W (3.2 kts) and 151.73°W (2.9 kts) exceed the corresponding meridional current components (2 kts and 2.6 kts, respectively) at these locations. The phase plot indicates that maximum semidiurnal surface currents in the shipping channel lag the surface currents near the eastern side of the inlet by approximately 1.5–2 hours. The tidal ellipses also provide clues as to the locations and phasing of the tide rips. The orientations of the ellipses suggest convergence during the flood tide at locations between 151.3°W and 151.4°W, between 151.5°W and 151.6°W, and near 151.7°W. These convergences correspond to the locations of the East Rip, Middle Rip, and West Rip, respectively. The orientations of the ellipses also suggest convergences occur during ebb tide between 151.4°W and 151.5°W (East Rip) and between 151.7°W and 151.8°W (West Rip). The absence of a prominent surface convergence in the middle of the transect suggests that the Middle Rip dissipates during the ebb tide.

There are three principal loci at which large amplitude (>2 psu) semidiurnal salinity signals are evident (Figure 8a). The most vertically extensive locus occurs on the western flank of the shipping channel at depths between 35–55 m and is associated with the base of the Middle Rip front. The local amplitude maximum near the eastern side of the inlet is associated with the East plume, whereas the local maximum above the western shoulder of the shipping channel near Kalgin Island is associated with the West Rip front. Note, however, that the width of these large amplitude signals is about 1–2 n mi. (1.82–3.64 km). Broadly speaking, the amplitude of the

semidiurnal salinity signal within the shipping channel exceeds the amplitude in shallower waters. The minimum amplitude for the semidiurnal salinity signal (<0.8 psu) occurs in the surface layer within the shipping channel. The relatively weak semidiurnal salinity signal at this location reflects the persistence of the Forelands plume. The companion phase plot (Figure 8b) shows that semidiurnal period changes in salinity near the eastern side of the inlet lead changes in the shipping channel by 2–3 hours. Comparison of the salinity phase plot with the surface current phase plot indicates that, across most of the transect, the maximum surface salinities occur approximately 2–3 hours after the maximum surface currents. It can be inferred from this relationship that the highest salinities occur near the end of the flood tide. Conversely, minimum salinities occur near the end of the ebb tide.

The general pattern of semidiurnal temperature signals (Figure 9a) is similar to the pattern of the semidiurnal salinity signals (compare Figure 8a). The largest amplitude semidiurnal temperature signal ($>0.8^{\circ}\text{C}$) occurs along the western flank of the shipping channel. Secondary amplitude maxima ($>0.5^{\circ}\text{C}$) occur in shallow water near Kalgin Island and at the seaward flank of the river plume along the eastern side of the inlet (compare with Figure 3). The amplitude minimum ($<0.2^{\circ}\text{C}$) occurs in the upper 5 m of the shipping channel. A secondary minimum occurs in shallow water adjacent to the eastern side of the inlet. The companion phases plot (Figure 9b) shows that semidiurnal temperature signal in the shipping channel lags the signal near the eastern side of the inlet by 3–4 hours. As expected, a comparison of the temperature phase plot with the salinity phase plot (compare Figure 9b) shows that the temperature maximum occurs roughly six hours (half a semidiurnal cycle) after the salinity maximum. This out-of-phase relationship implies that warm temperatures are associated with fresher waters and cool temperatures are associated with more saline waters.

The general pattern of semidiurnal transmissivity signals (Figure 10a) is somewhat similar to the mean transmissivity conditions (compare Figure 6). The least variation occurs where the mean transmissivity is lowest: along the western flank of the shipping channel and between the shipping channel and the eastern side of the inlet. The largest amplitude semidiurnal transmissivity signal occurs in the shallow water next to Kalgin Island. Moderate amplitude ($>25\%$) semidiurnal transmissivity signals also occur near the bottom and surface in the middle of the shipping channel and on the seaward flank of the Kenai and Kasilof River plume. The companion phase plot (Figure 10b) shows that large phase gradients occur along the western flank of the shipping channel and midway between the shipping channel and eastern side of the inlet, whereas small phase gradients occur within the middle portion of the shipping channel. Comparison of the transmissivity amplitude with the mean transmissivity plot (compare Figure 6) indicates that high suspended sediment concentrations and the least variability in concentration occur in association with large phase gradients and that low suspended sediment concentrations are associated with small phase gradients. Moreover, comparison of the transmissivity phase plot with the salinity phase plot (compare Figure 8b) indicates that within much of the shipping channel, the phase of the two properties differ by less than an hour. Stated another way, the flood tide carries relatively clear, saline water northward and the ebb tide carries relatively turbid, fresh water southward.

Diurnal variability

Mean diurnal surface current tidal ellipses and phases along the transect are shown in Figure 11. In general, the diurnal amplitudes are less than half the semidiurnal amplitudes. As was the case for the semidiurnal surface currents, the largest amplitude diurnal currents (~ 1.5 kts) occur within the shipping channel. Zonal (east-west) components of the diurnal surface currents are largest on

the west side of the transect and midway between the shipping channel and eastern side of the inlet. The phase plot indicates that maximum diurnal surface currents in the shipping channel lag the diurnal surface currents near the eastern side of the inlet by about 2 hours. The phases of maximum diurnal currents at the three westernmost locations and at 151.37°W differ substantially from the phases at the other locations.

The largest amplitude diurnal salinity signal (>1 psu) occurs along the bottom of the shipping channel (Figure 12a). The smallest amplitude diurnal signals (<0.4 psu) occur next to Kalgin Island, in the surface (0–5 m) layer within the shipping channel, and roughly midway between the shipping channel and eastern side of the inlet. The phase plot (Figure 12b) shows that across most of the transect, except near the western and eastern side of the inlets, the phase differential is typically less than 4 hours (1/6 diurnal cycle).

The plot of the amplitude of the diurnal temperature signal (Figure 13a) indicates that the largest amplitude temperature signals ($>0.4^{\circ}\text{C}$) occur in the upper meter or two of the Forelands plume and East plume. The phase plot (Figure 13b) indicates that these shallow temperature maxima occur in the late afternoon (1600–1800 hrs local time), suggesting that these surface signals result from solar heating. There is also a ~10-m thick layer at the bottom of the shipping channel that exhibits a $>0.3^{\circ}\text{C}$ diurnal variation. Across much of the remainder of the transect, the amplitude of the diurnal temperature signal is $<0.2^{\circ}\text{C}$.

The largest amplitude diurnal variation in transmissivity ($>20\%$) occurs through much of the water column in the middle of the shipping channel (Figure 14a). The diurnal signal is smallest near the bottom the shipping channel and midway between the shipping channel and the eastern side of the inlet. The phase plot (Figure 14b) shows that phase is relatively constant at mid-depths in the center of the shipping channel. However, across most of the remainder of the transect, there are prominent horizontal and vertical phase gradients.

Discussion

There are a number of qualifications to the observational data sets that should be kept in mind when reviewing and interpreting these data. In order to estimate instantaneous conditions, it was assumed that the time variations of the field variables at any location on the section plane could be represented by linear combinations of diurnal (K1) period and semidiurnal (M2) period sinusoidal functions, a trend, and constant offset. The tidal amplitudes and corresponding phase estimates were derived from relatively few measurements (nine occupations of the transect) acquired during a 26-hour period. This limitation is most severe at the endpoints of the transect because the times between repeat measurements were greatest. The temperature and salinity observations reflect mid-summer conditions, that is, conditions that are approaching the warmest and freshest values, as well as strongest gradients, of their seasonal cycles. Additionally, the observations were acquired during the beginning of the spring tide portion of the fortnightly tidal cycle. Spring tides are characterized by stronger currents and larger tidal ranges than are neap tides. Wind and wave effects are not represented because observations were acquired during a period of light winds and calm seas.

The preceding descriptions of hydrography and surface currents provide important clues as to the dominant physical forces governing circulation and the evolution of fronts in Cook Inlet. Strong convergences and shears in the surface currents characterize Cook Inlet tide rips. The temporal and spatial occurrences of convergence zones are depicted in a plot the zonal derivative of the

east-west surface velocity component ($\partial u/\partial x$) for each time t . Convergences occur when and where $\partial u/\partial x < 0$, assuming that $\partial v/\partial y$ is negligible (Figure 15). The surface current vector overlay shows that the strong West Rip convergence zone results from the large east-west (u) velocity component at 151.73°W relative to the u components at 151.77°W and 151.7°W (see also Figure 7). The West Rip oscillates around $\sim 151.73^\circ\text{W}$, with strongest convergences occurring within a few hours either side of slack water. The Middle Rip convergence resides between $\sim 151.53^\circ\text{W}$ and 151.6°W with the strongest convergences occurring during much of the flood and continuing through the beginning of the ebb. The East Rip convergence generally occurs during the ebb between 151.5°W and 151.43°W . Slightly stronger convergences are evident near the eastern shore during the flood. Overall, the instantaneous widths of the convergence zones are $\sim 2\text{--}4$ n mi with the strong West Rip convergence exhibiting an instantaneous width of about 2 n mi.

The underlying constraint on the location of the surface current shear zones can be deduced from the plots of the tidal ellipses (Figure 7 and Figure 11) which show that the speeds of tidal currents vary with the water depth. That is, the faster along-channel currents generally occur in deeper water and, conversely, the slower currents occur in shallower water. The depth dependence of the tidal current speeds indicates that frictional effects imparted to the water column by the channel floor are important in determining the characteristics of the tidal flow field. The relevant dynamics are those governing turbulent flow in an open channel. A very simple representation of this relationship (steady state and no rotation) states that the current velocity, V , is proportional to the square root of the channel depth, H ,

$$V \propto H^{1/2} \quad \text{(equation 5)}$$

The cross-channel derivative of equation 5

$$\partial V/\partial x \propto H^{-1/2} \partial H/\partial x \quad \text{(equation 6)}$$

indicates that prominent velocity shears should occur where the cross-channel bottom slope is large. The temporal evolution of the along-channel velocity shear ($\partial v/\partial x$) field (Figure 16) shows this to generally be the case. The largest magnitude shears occur over the steep western flank of the shipping channel during ebb tide. Somewhat weaker magnitude shears occur near the eastern flank of the shipping channel between 151.63°W and 151.57°W . Even weaker magnitude shears occur near 151.43°W . The locations of these three shear zones correspond to the respective locations of the West, Middle, and East rips as inferred from the velocity convergence plot. From a temporal perspective, the magnitudes of the velocity shears tend to be larger during the latter half of the flood and ebb.

It is readily apparent from comparisons of the time evolution of the surface salinity field (Figure 17) with the corresponding convergence and shear plots (see Figures 15 and 16) that salinity fronts are associated with the West Rip and Middle Rip convergence and shear zones. The East Rip, however, does not exhibit significant zonal salinity gradients at any time during the sampling period. The strong salinity front at the flank of the east plume exhibits its greatest offshore extent near the end of the ebb and its closest approach to the eastern shore near the end of the flood. The zonal migration of each of these salinity fronts appears to be roughly 1–2 n mi.

The plot of the mean density-driven currents and mean surface currents (see Figure 5) and the M2 tidal currents (see Figure 7) provide a context for understanding the influence of freshwater inputs to Cook Inlet on the variability of the (vector) surface currents illustrated in Figures 15–17. The mean density-driven southward flow between 151.7°W and 151.6°W will augment tidal ebb

currents and oppose tidal flood currents. The mean density-driven northward flows east of 151.6°W and west of 151.7°W will augment tidal flood currents and oppose tidal ebb currents. The result is that where mean density-driven flow is northward (along the eastern shore and near Kalgin Island), the onset of northward tidal flow (flood tide) occurs earlier and has longer duration than the onset and duration of northward tidal flow where mean density-driven flow is southward (in the shipping channel). Conversely, where mean density-driven flow is southward (in the shipping channel), the onset of southward tidal flow (ebb tide) occurs earlier and has longer duration than the onset and duration of southward tidal flow along the eastern shore and near Kalgin Island.

The results presented above can be generalized to qualitatively describe conditions at other times during the fortnightly and seasonal cycles. It can be inferred from the asymmetry of the two semidiurnal tidal cycles during the sampling period (currents were weaker on 9 August than on 10 August) that, over the fortnightly tidal cycle, tide rips (current shears and convergences) and property gradients (temperature, salinity, suspended sediments) will be stronger during the spring tide and weaker during the neap tide. Because cross-channel freshwater (density) gradients alter the phases of tidal currents, it can be inferred from the seasonal cycle of freshwater inputs to Cook Inlet (high inputs in summer and low inputs in winter) that density-driven currents will be weaker and the phases of the tidal currents will be more uniform across the inlet during winter than in summer.

The results can also be generalized to infer rip locations throughout Cook Inlet. Equation 6, along with Figures 15 and 16, indicate that strong tide rips are associated with the steep bathymetry. Figure 18 shows bathymetric gradients computed from digital bathymetry of the Cook Inlet region (see Figure 1). The steep bathymetry lying immediately east of Kalgin Island and extending northward through the Forelands and southwestward to the latitude of Ninilchik is associated with the West Rip. The bathymetric gradients associated with the Middle Rip and East Rip are also evident, but less prominent. Strong bathymetric gradients exist to the west of Kalgin Island. A radar image of ice distribution in central Cook Inlet on 8 February 2000 (Figure 19) supports the generalization that rips/fronts (ice edges) are well correlated with bathymetric gradients.

In summary, the results from this study suggest that Cook Inlet numerical circulation models require accurate, high-resolution bathymetry to correctly locate fronts (rips). Additionally, these models need to be fully three-dimensional, incorporating buoyancy (temperature and salinity) effects at seasonal to semidiurnal time scales to improve their forecasting skill.

References

- Burbank, D. C. 1977. Circulation studies in Kachemak Bay and Lower Cook Inlet. Trasky, L. L. L. B. Flagg D. C. Burbank ed(s). vol. III. Alaska Department of Fish and Game. Anchorage, AK. pp. 207.
- Whitney, J. 1994. Past experience with spill response in Cook Inlet. Anchorage, AK: ISCOI, NOAA, Hazardous Materials Response and Assessment Division.

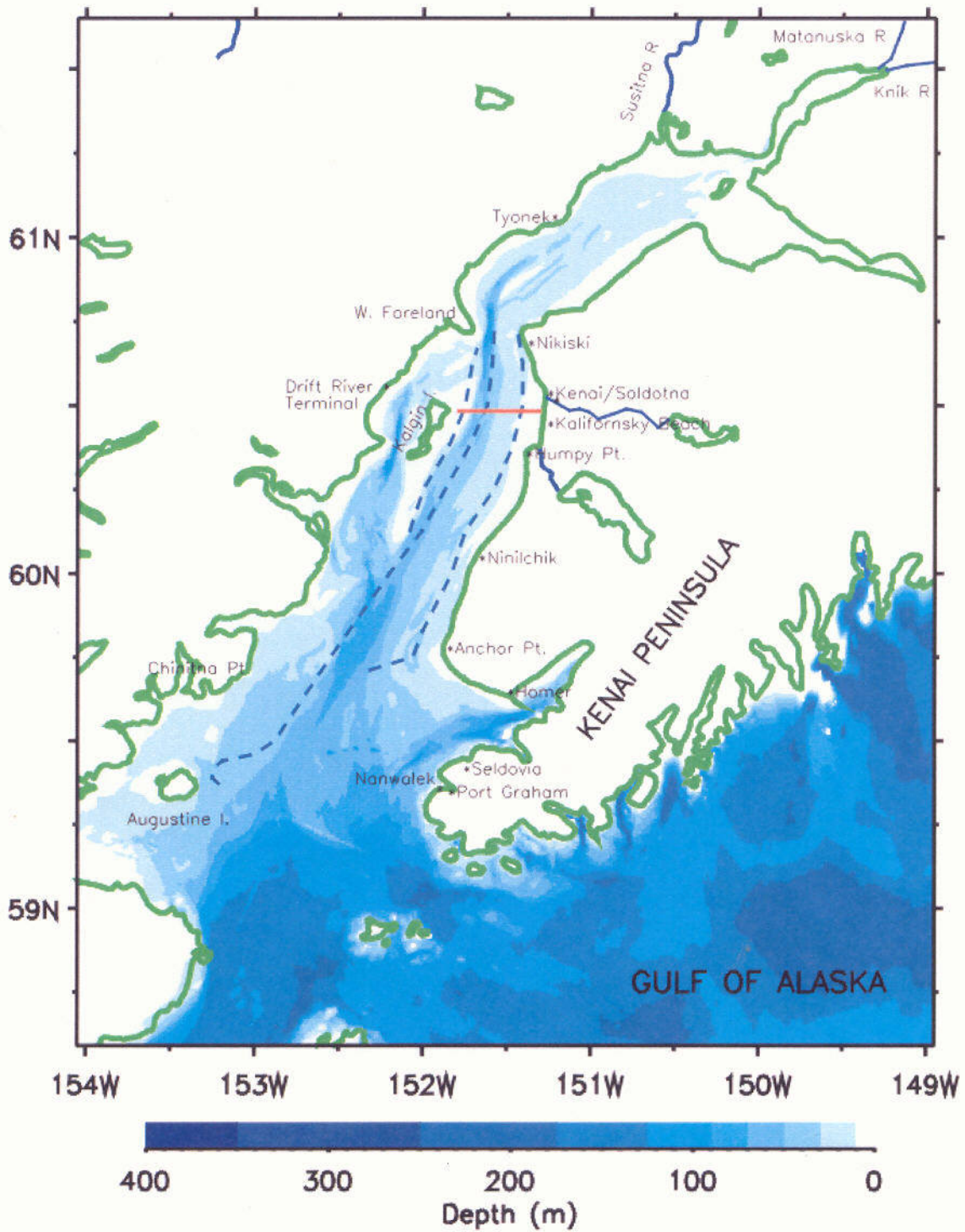


Figure 1. Bathymetric map and place names of Cook Inlet, Alaska. The location of the hydrographic section is shown as a red line.

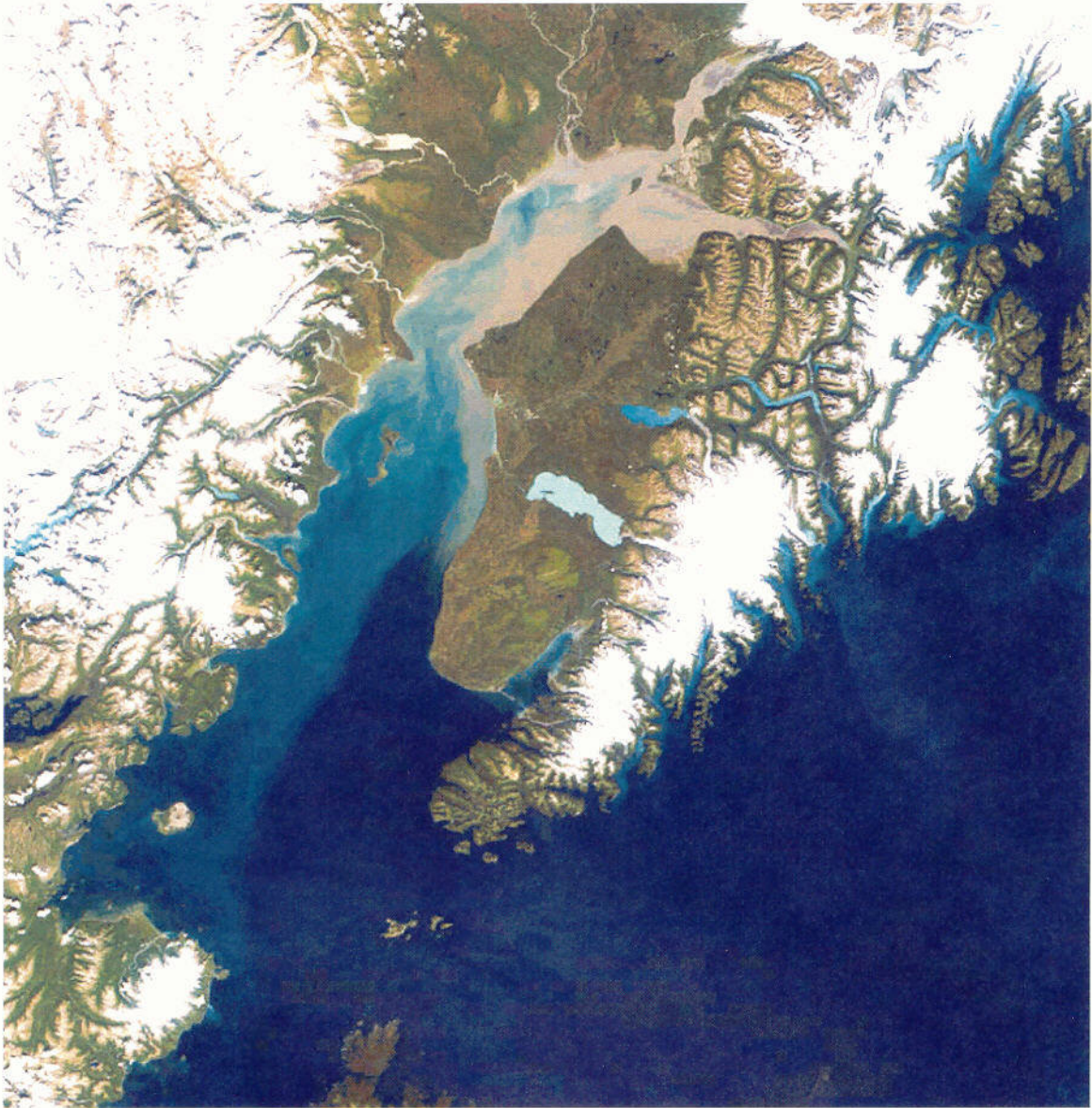


Figure 2. MODIS true color image of Cook Inlet acquired 2 September 2002.

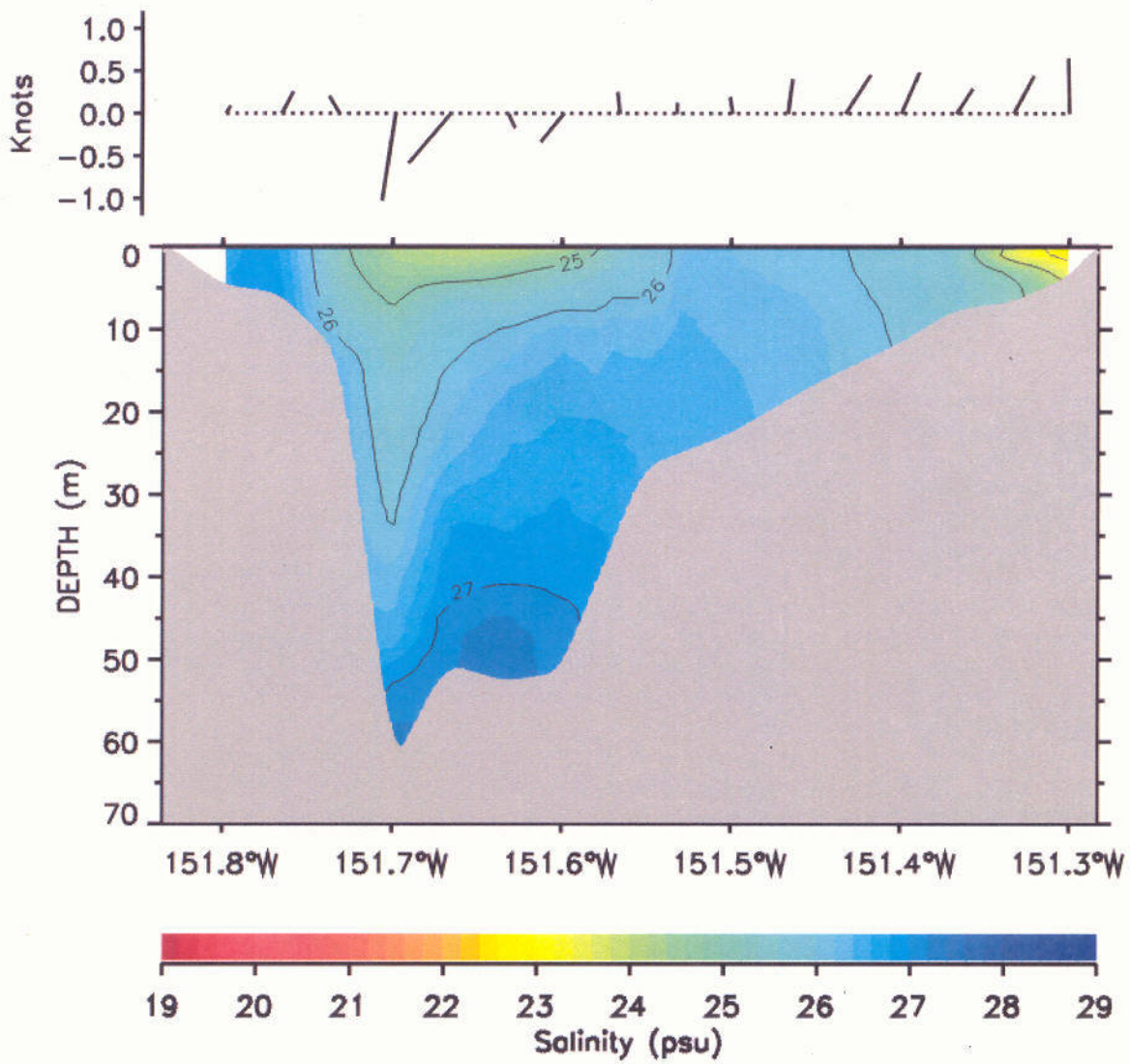


Figure 3. (Top) Mean surface currents vectors across section. Northward flow is up, southward flow is down. (Bottom) Mean salinity across section. Contour interval is 1.0 psu.

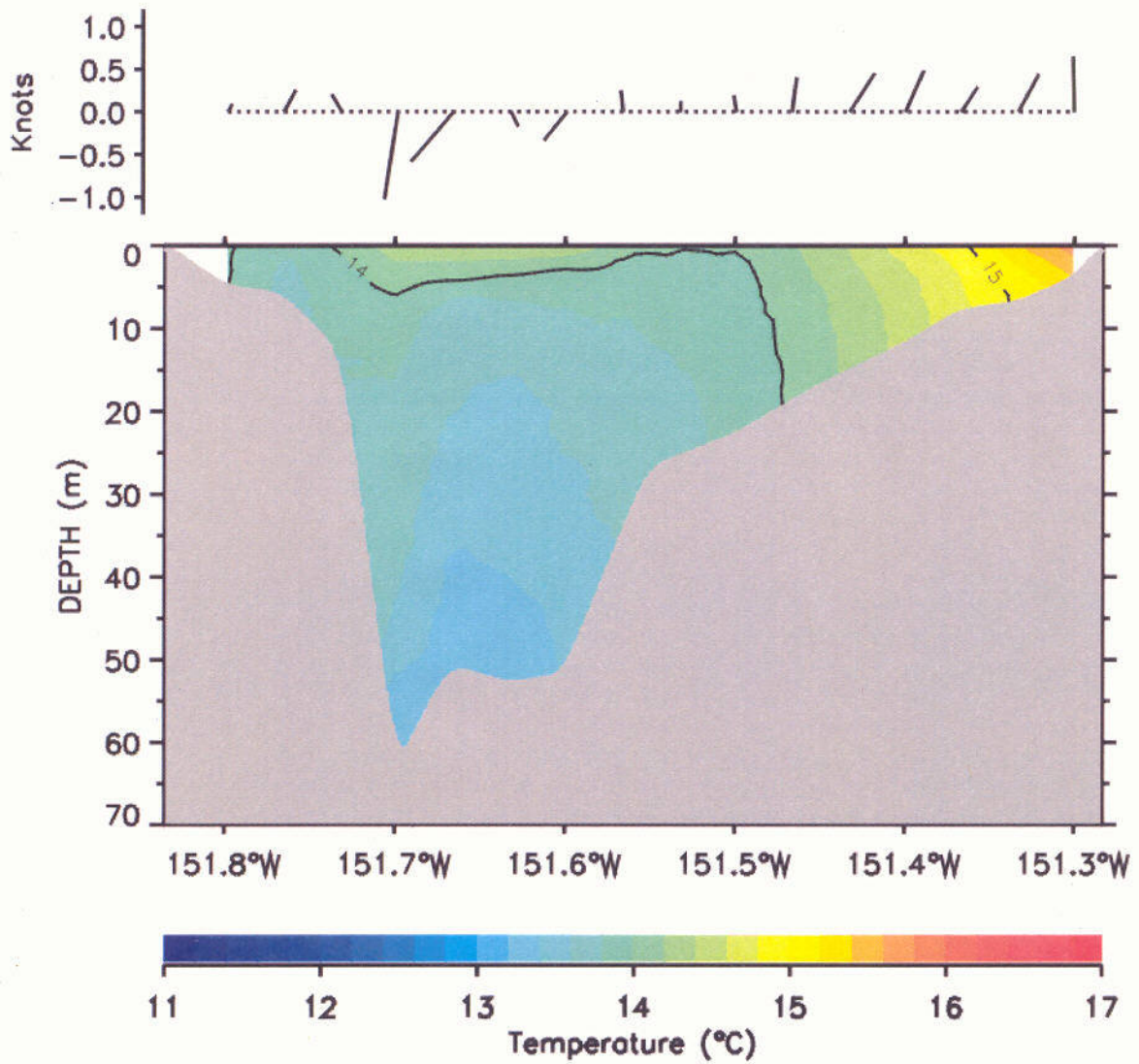


Figure 4. (Top) Mean surface currents vectors. Northward flow is up, southward flow is down. (Bottom) Mean temperature across section. Contour interval is 1.0° C.

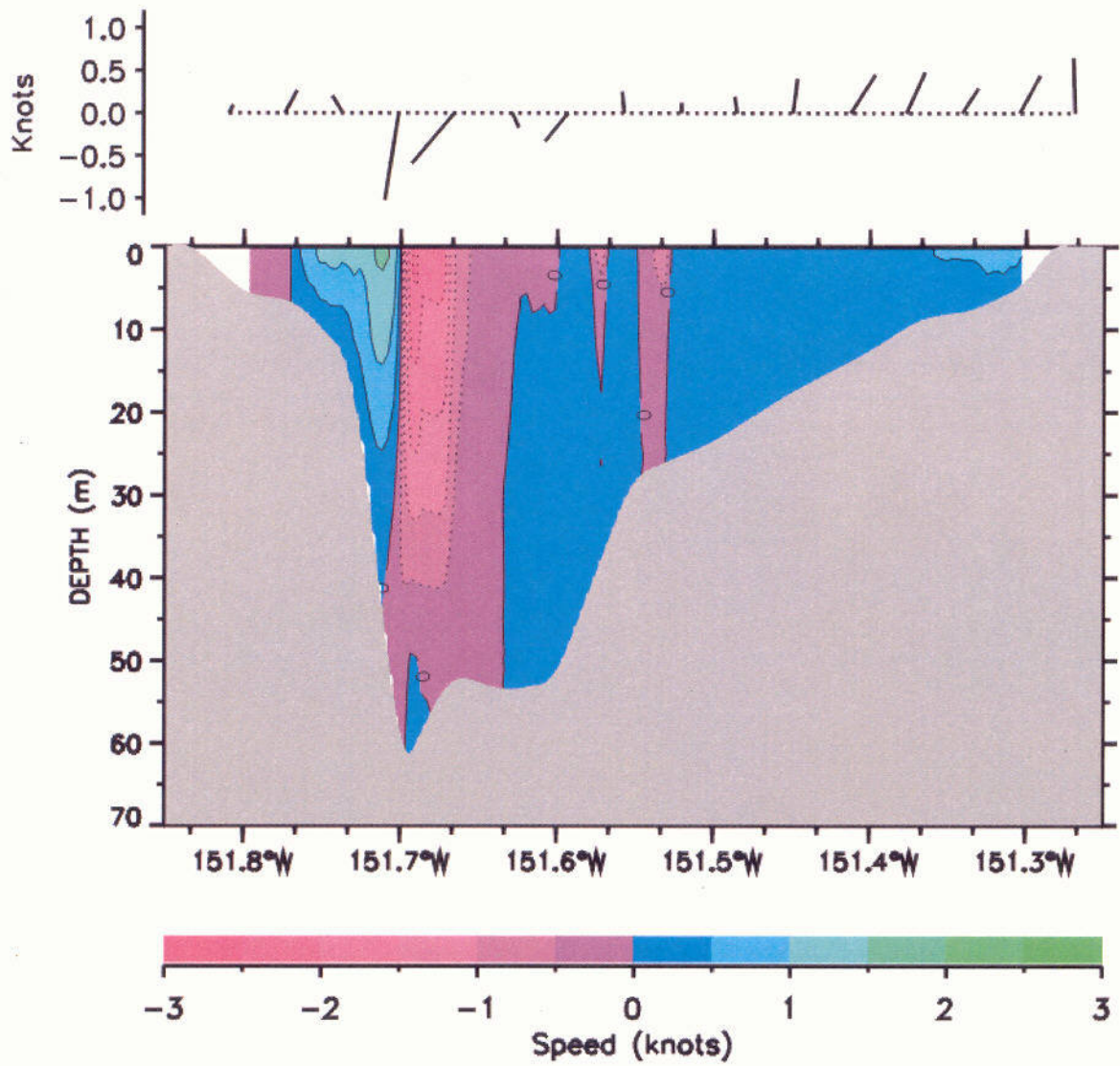


Figure 5. (Top) Mean surface currents vectors. Northward flow is up, southward flow is down. (Bottom) Mean baroclinic geostrophic velocity across section. Positive speeds are northward. Contour interval 0.5 kt.

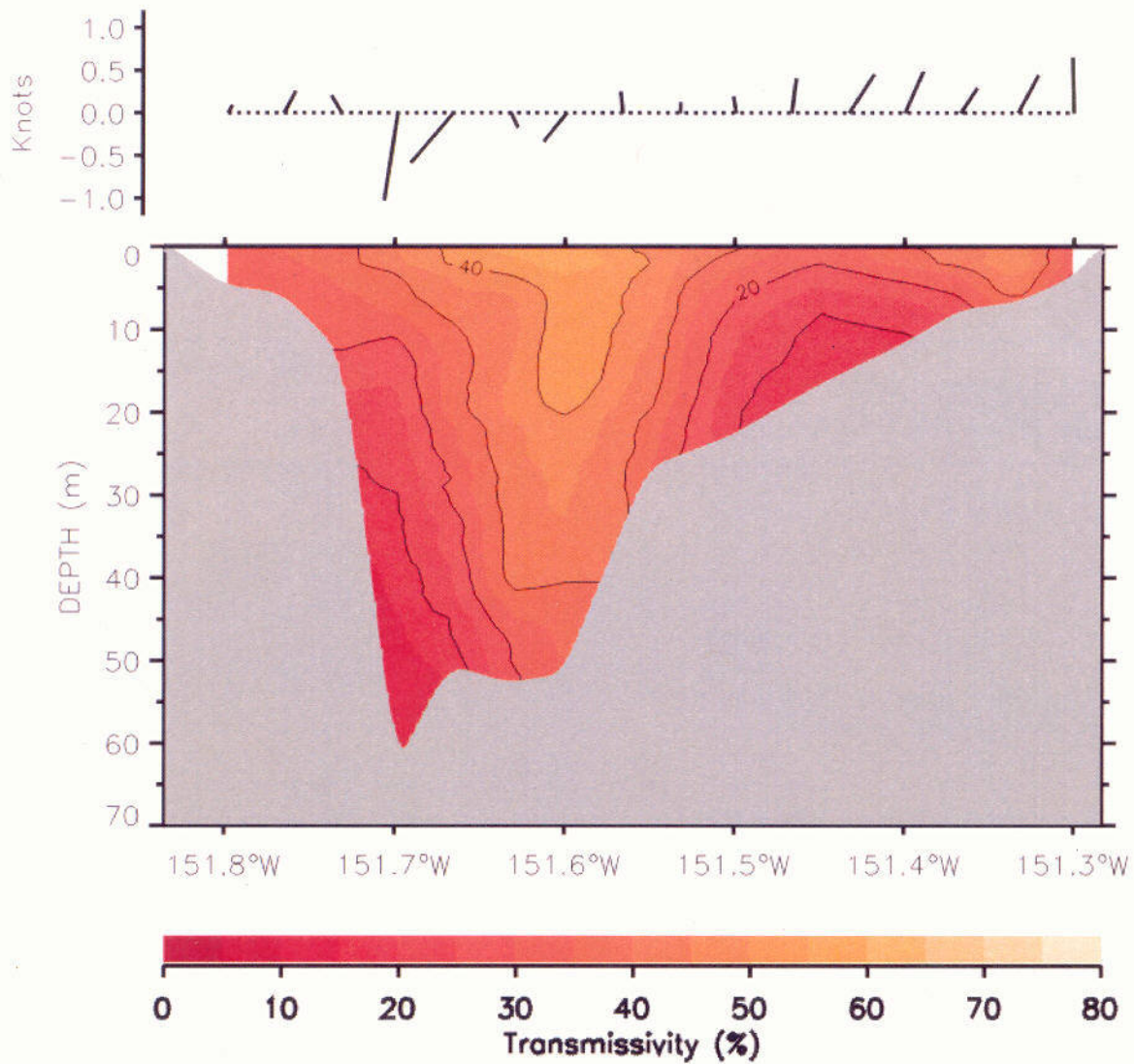


Figure 6. (Top) Mean surface currents vectors. Northward flow is up, southward flow is down. (Bottom) Mean transmissivity across section. Contour interval is 10%.

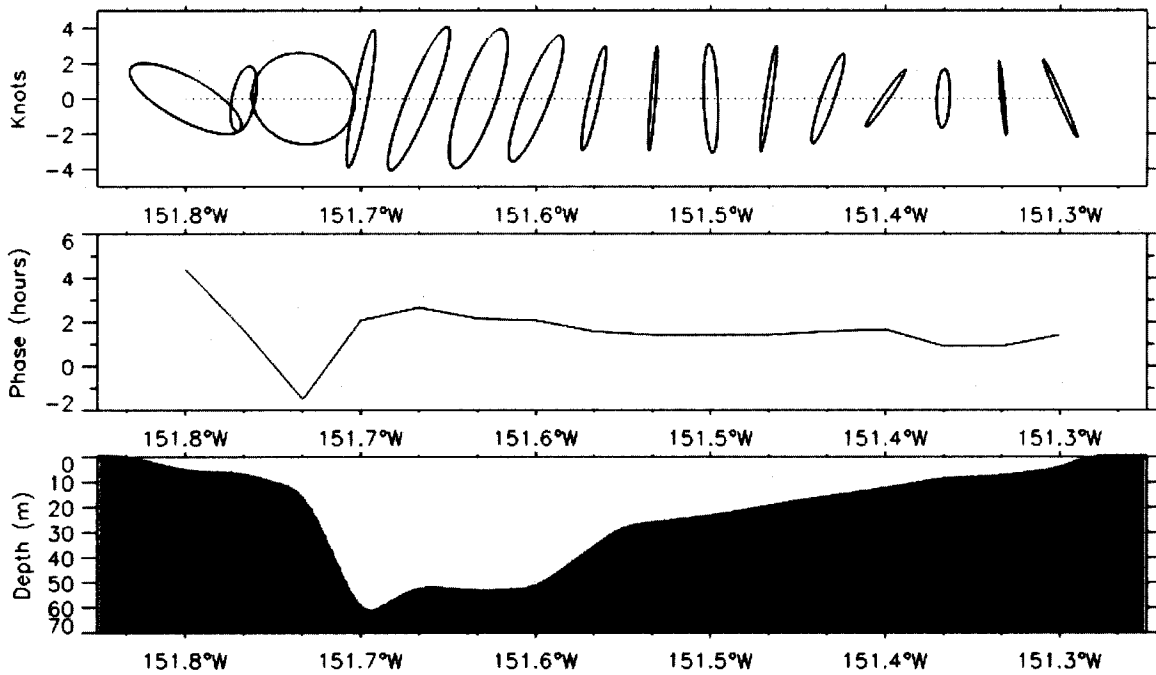


Figure 7. (Top) Semidiurnal (M2) tidal ellipses. Northward flow is up, southward flow is down. (Middle) Phase of semidiurnal tidal currents. Phase is relative to 00 hours, 9 August 2003 local time. (Bottom) Bottom depth profile along section.

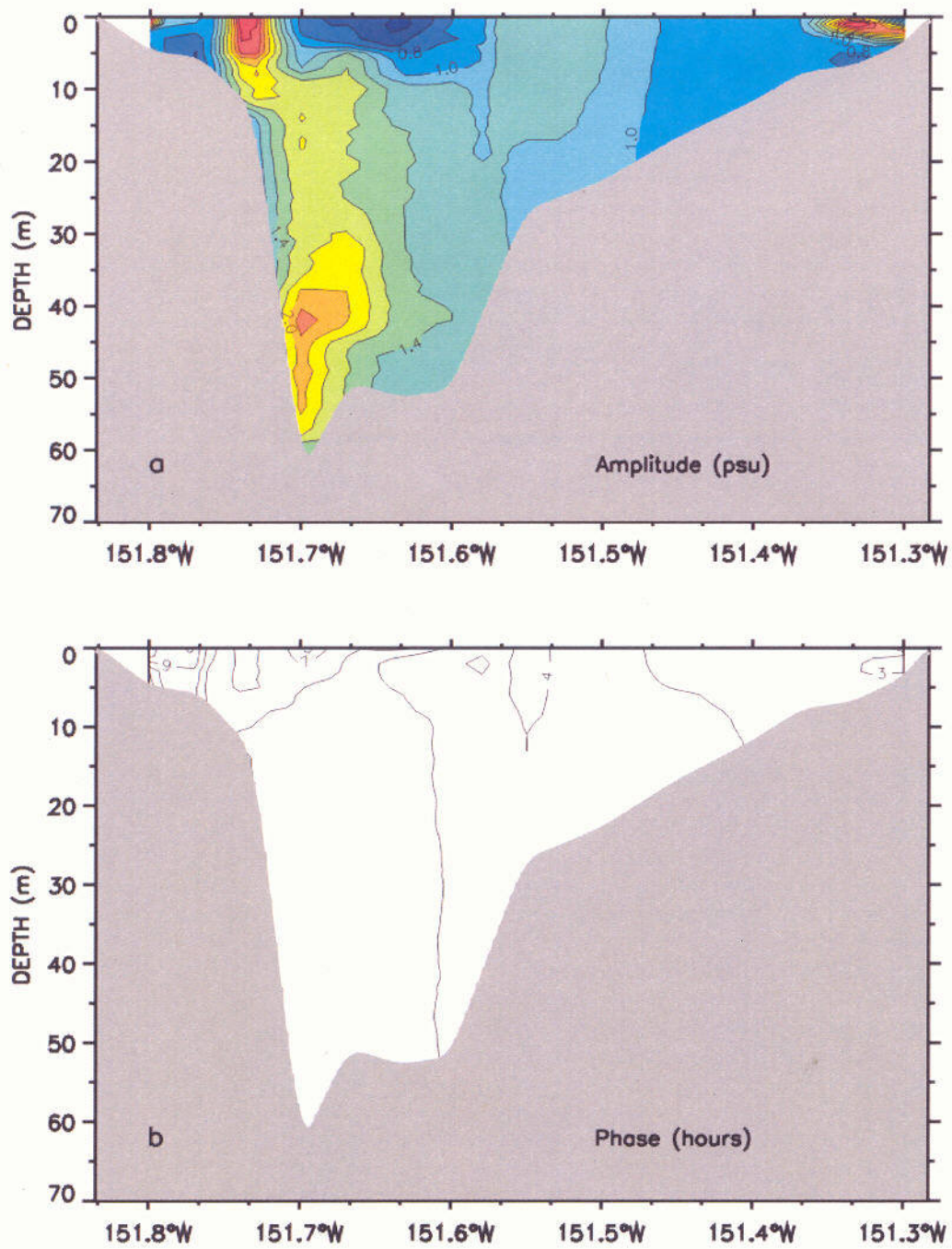


Figure 8. a) Amplitude of semidiurnal salinity signal. Contour interval is 0.2 psu. b) Phase of semidiurnal salinity signal relative to 00 hours, 9 August 2003 local time. Contour interval is 1.0 hours.

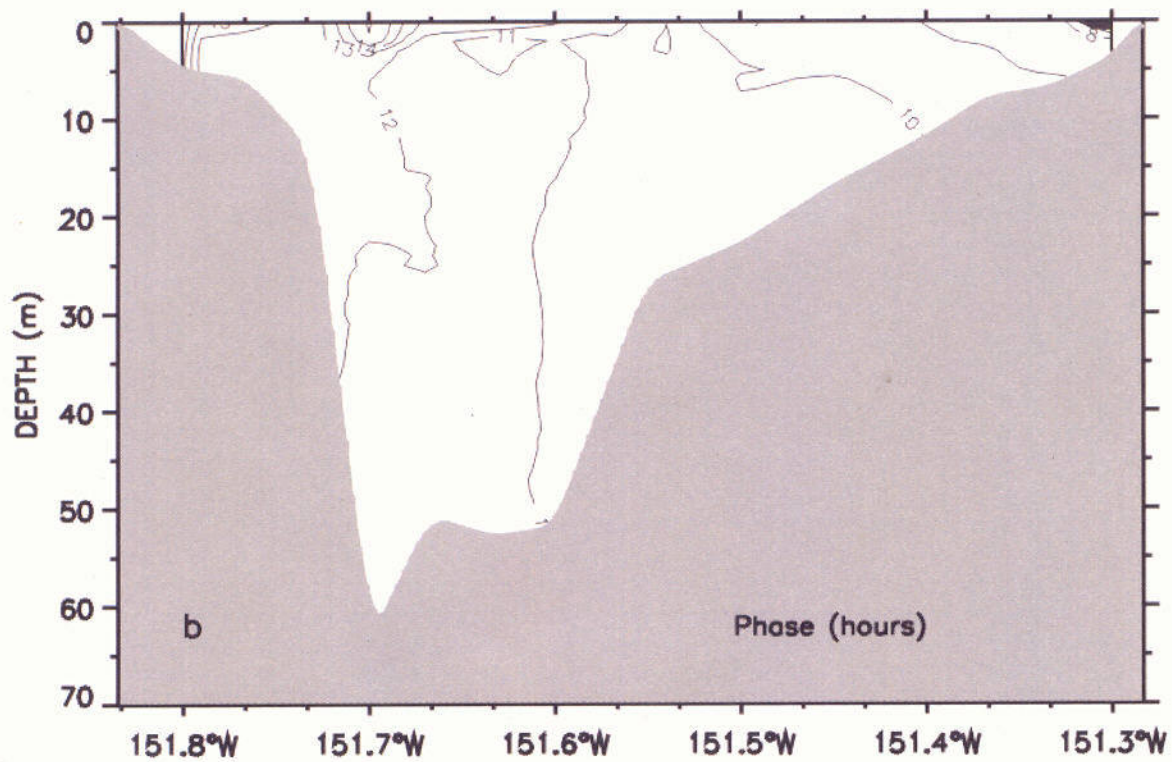
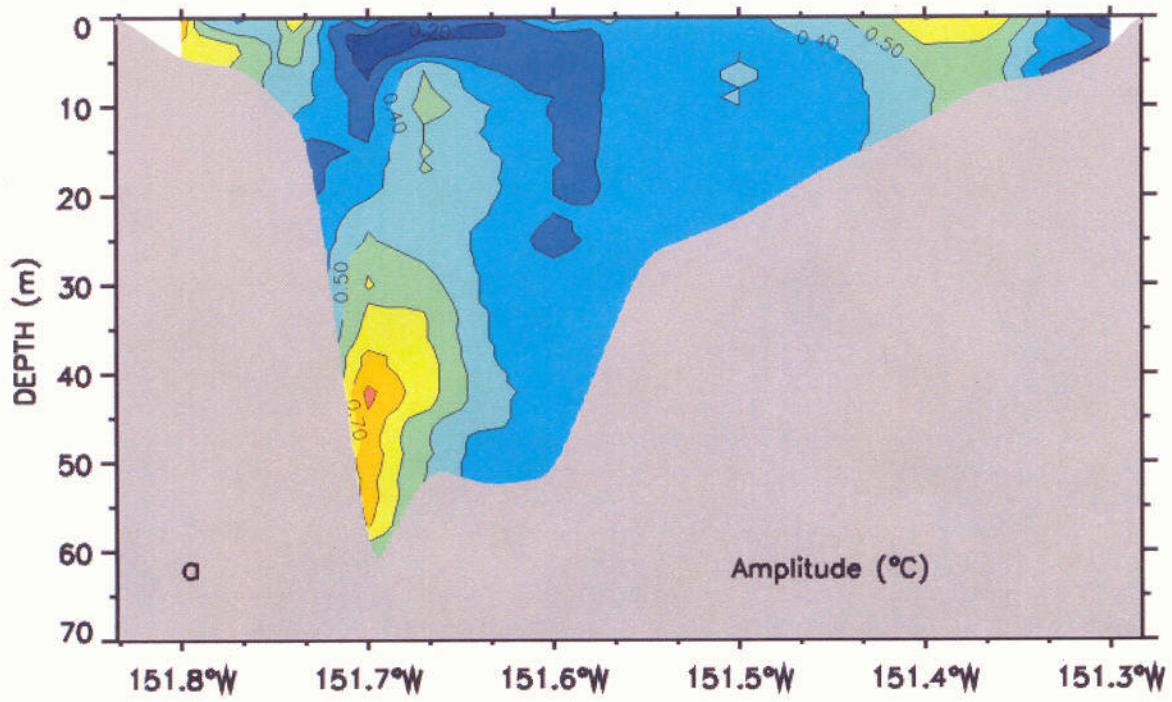


Figure 9. a) Amplitude of semidiurnal temperature signal. Contour interval is 0.1°C. b) Phase of semidiurnal salinity signal relative to 00 hours, 9 August 2003 local time. Contour interval is 1.0 hours.

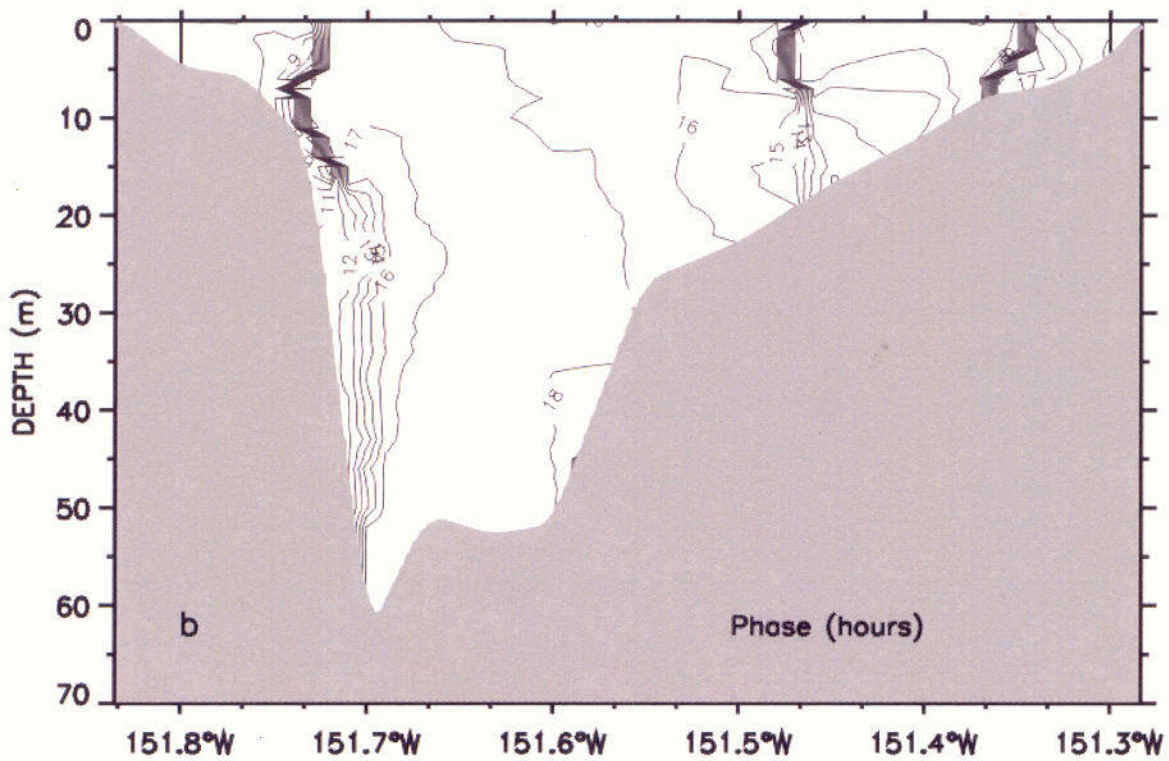
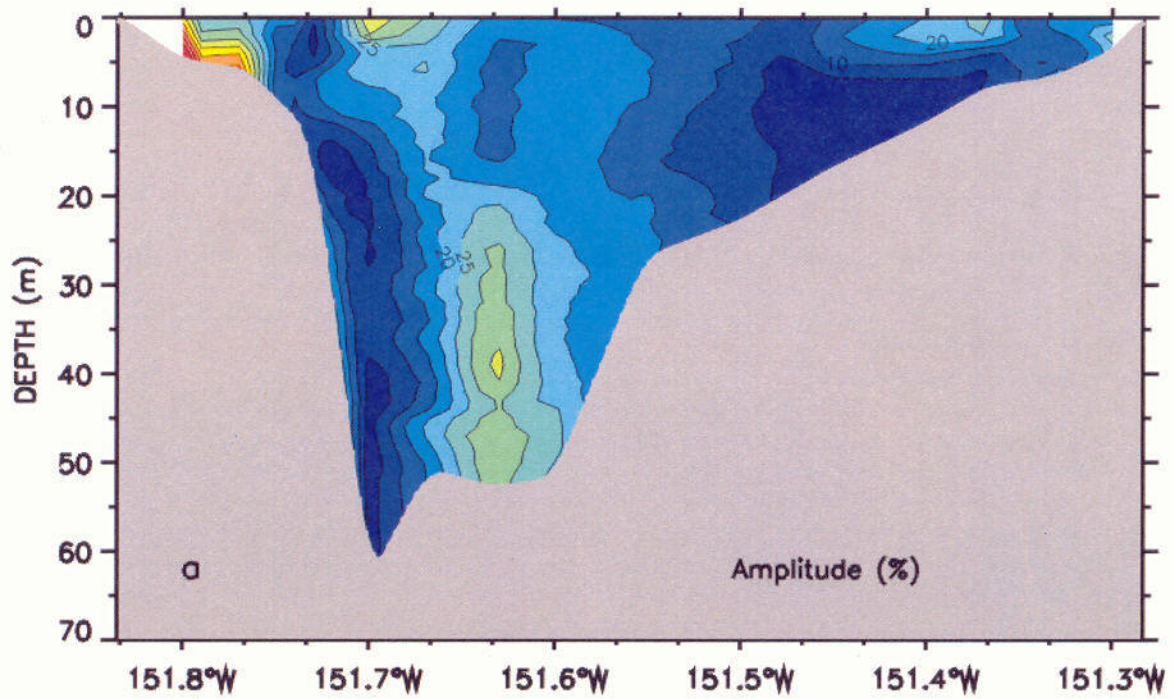


Figure 10. a) Amplitude of semidiurnal transmissivity signal. Contour interval 5%. b) Phase of semidiurnal salinity signal relative to 00 hours, 9 August 2003 local time. Contour interval is 1.0 hours.

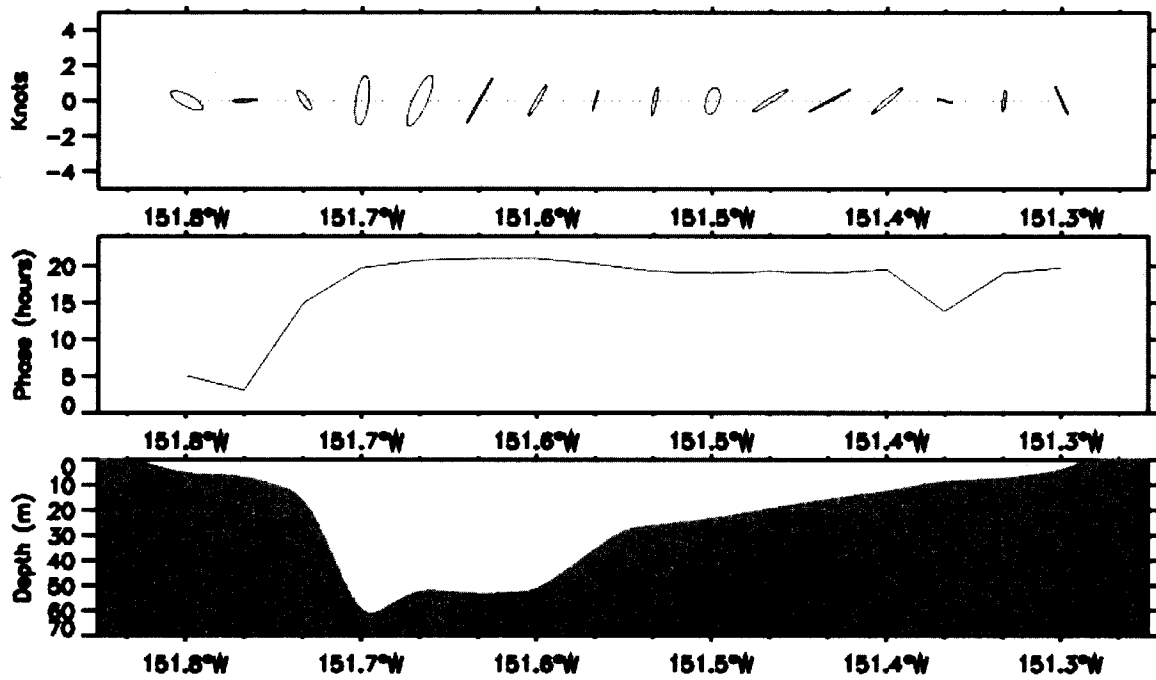


Figure 11. (Top) Diurnal (K1) tidal ellipses. Northward flow is up, southward flow is down. (Bottom) Phase of semidiurnal tidal currents. Phase is relative to 00 hours, 9 August 2003 local time. (Bottom) Bottom depth profile along section.

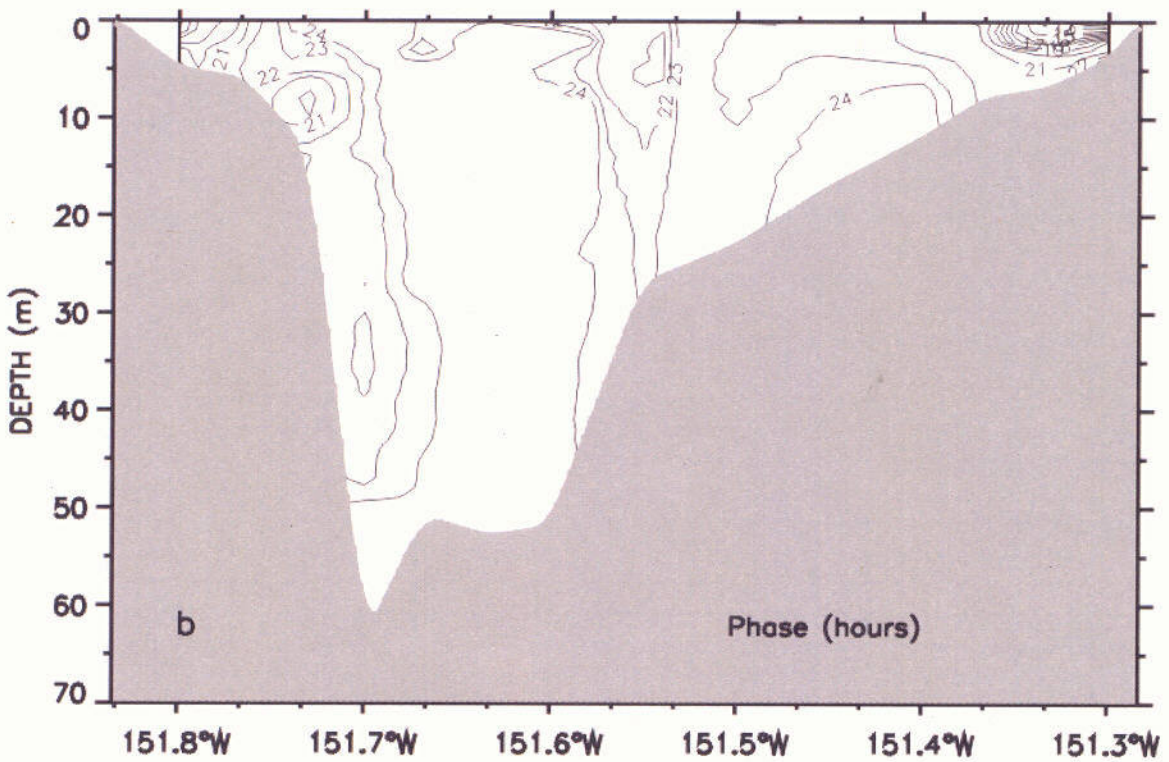
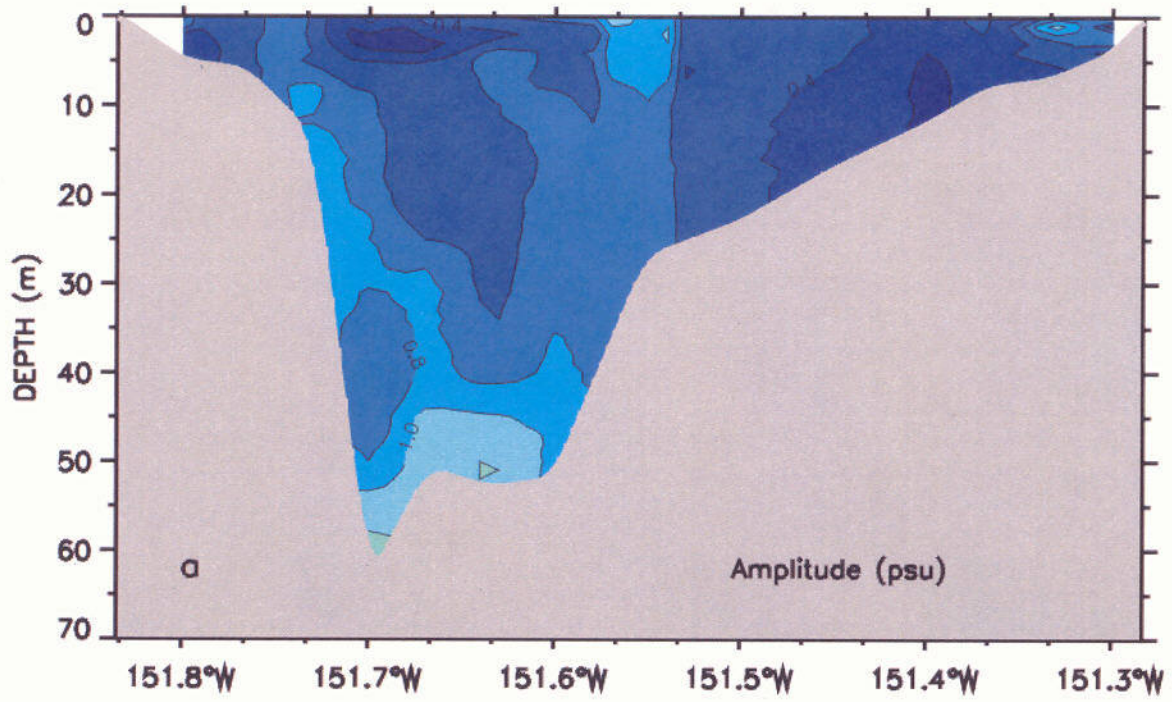


Figure 12. a) Amplitude of diurnal salinity signal. Contour interval is 0.2 psu. b) Phase of diurnal salinity signal relative to 00 hours, 9 August 2003 local time. Contour interval is 1 hour.

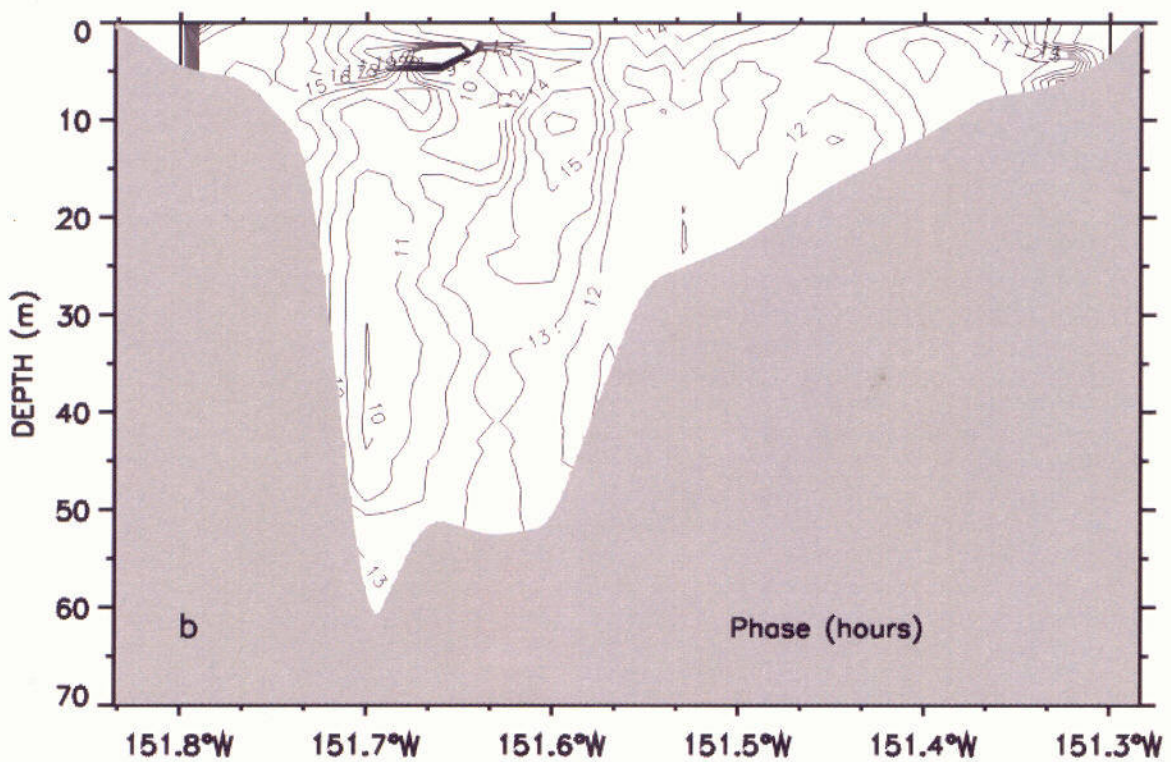
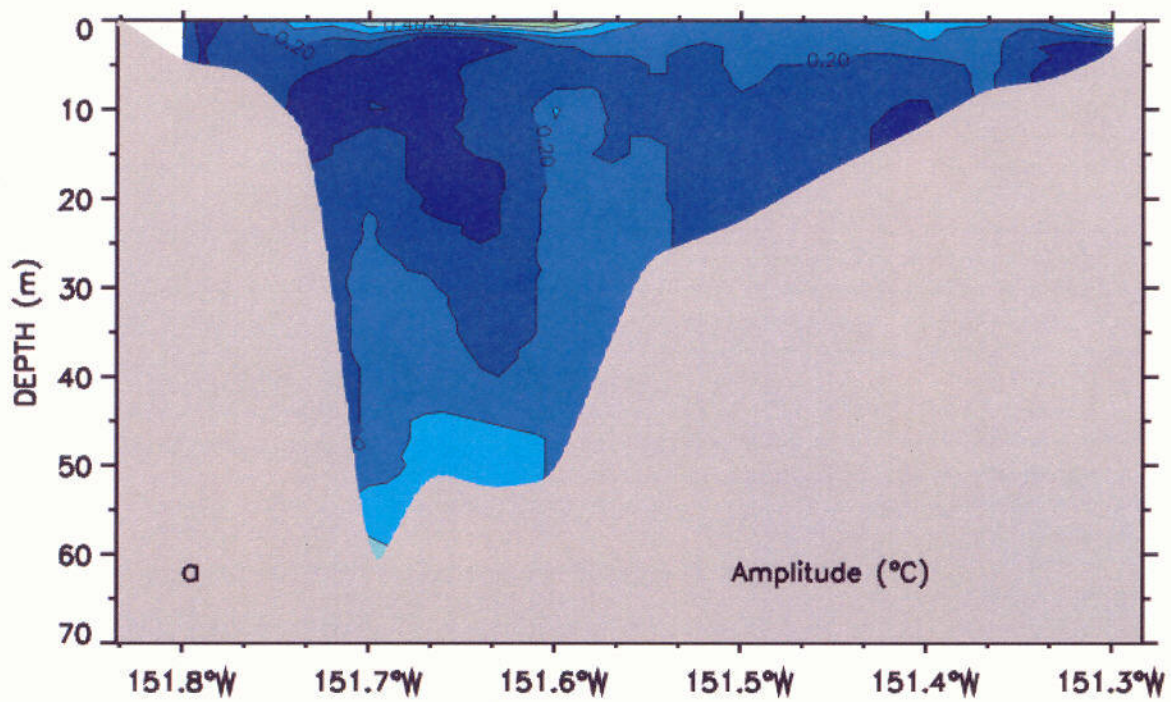


Figure 13. a) Amplitude of diurnal temperature signal. Contour interval is 0.1° C. b) Phase of diurnal salinity signal relative to 00 hours, 9 August 2003 local time. Contour interval is 1 hour.

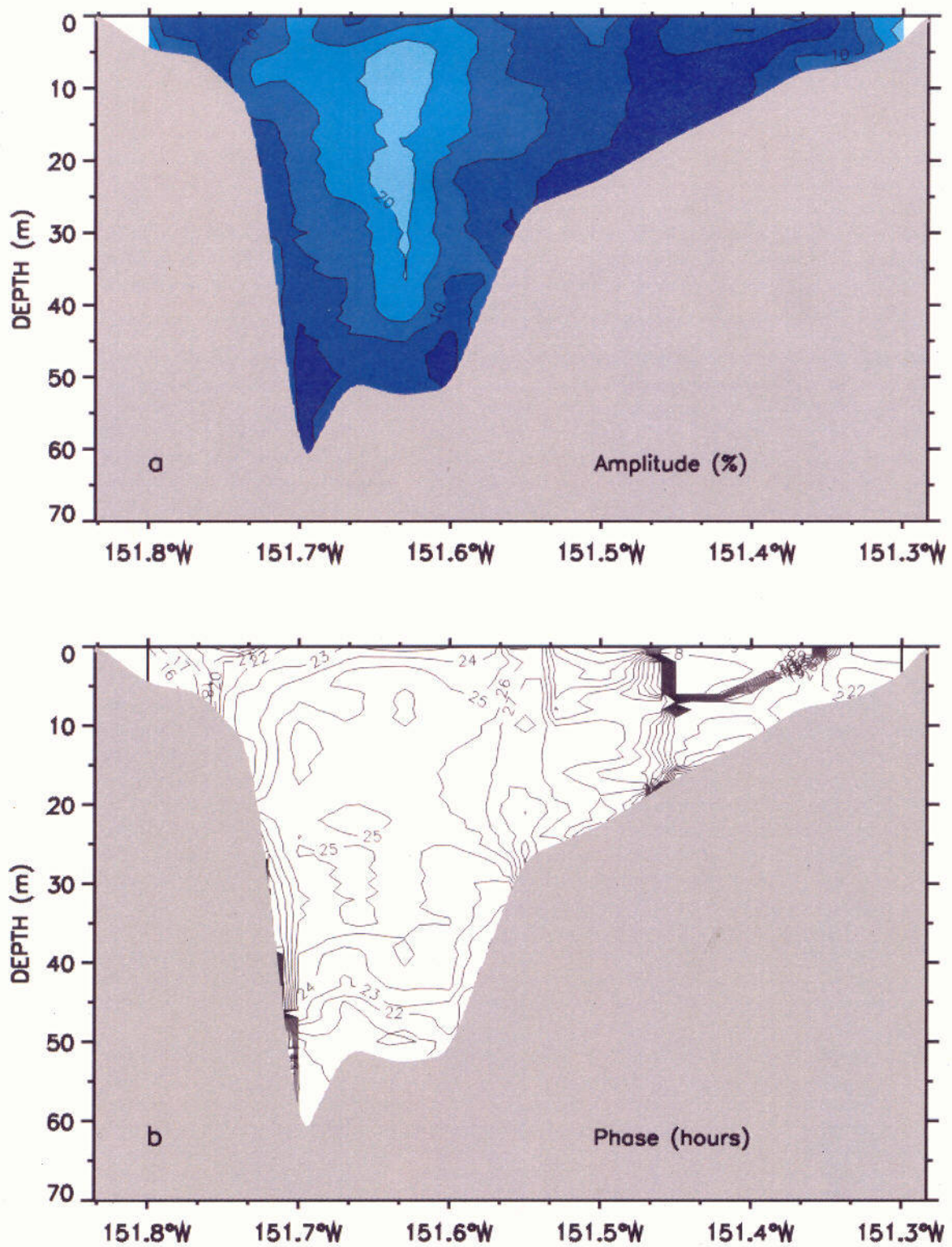


Figure 14. a) Amplitude of diurnal transmissivity signal. Contour interval 5%. b) Phase of diurnal salinity signal relative to 00 hours, 9 August 2003 local time. Contour interval is 1 hour.

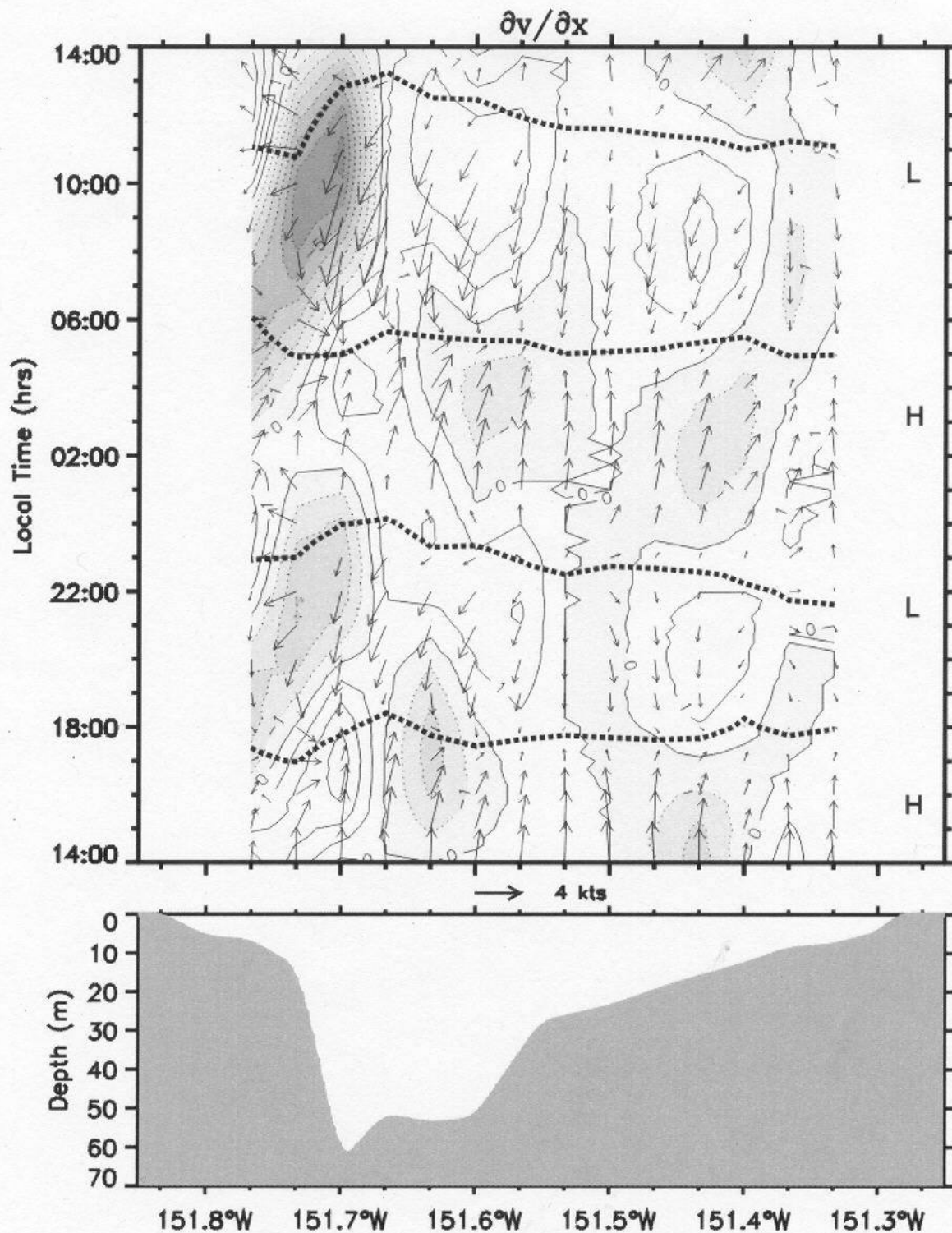


Figure 15. (Top) Time-longitude plot of cross-channel surface current divergence ($\partial u / \partial x$). Contour interval is $1 \times 10^{-4} \text{ s}^{-1}$. Convergence ($\partial u / \partial x < 0$) is shaded. Divergence ($\partial u / \partial x > 0$) is not shaded. Surface current vectors are shown. Thick dotted lines denote slack water (northward and southward current components are zero). Occurrences of (H)igh and (L)ow tides indicated on right side of plot. (Bottom) Bottom depth profile along section.

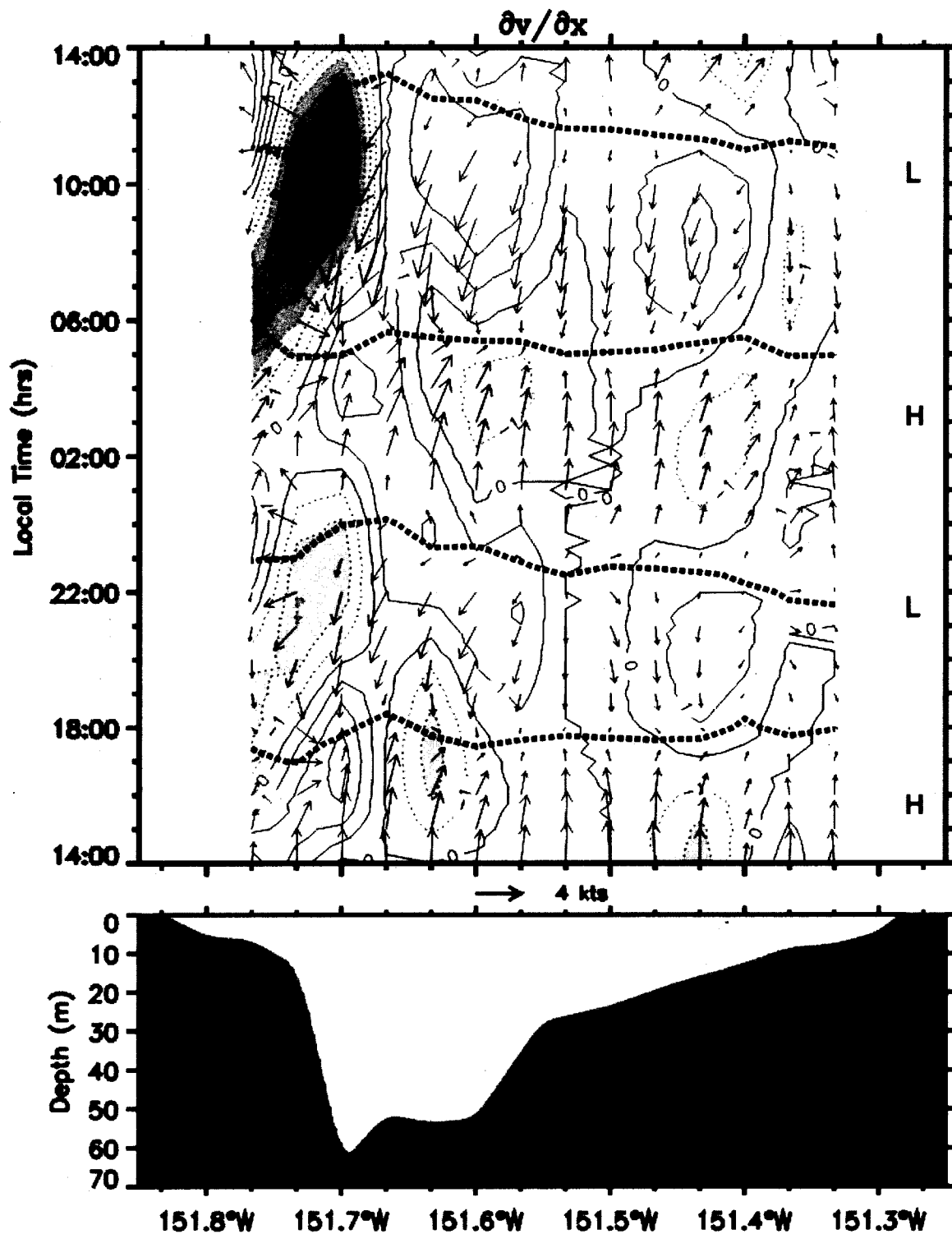


Figure 16. (Top) Time-longitude plot of along-channel surface current shear ($\partial v / \partial x$). Contour interval is $1 \times 10^{-4} \text{ s}^{-1}$. Negative shears ($\partial v / \partial x < 0$) are shaded. Surface current vectors are shown. Thick dotted lines denote slack water (northward and southward current components are zero).

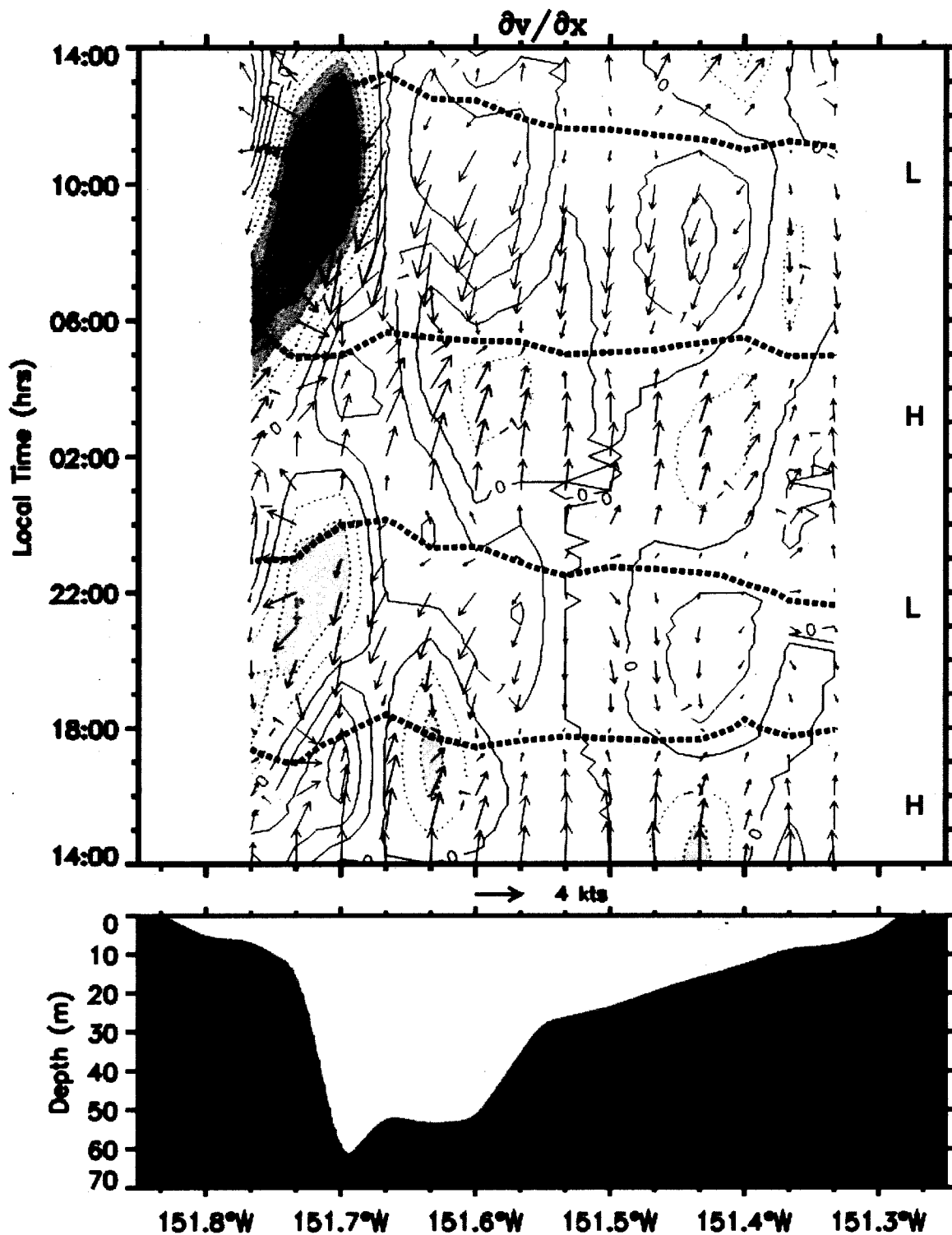


Figure 16. (Top) Time-longitude plot of along-channel surface current shear ($\partial v / \partial x$). Contour interval is $1 \times 10^{-4} \text{ s}^{-1}$. Negative shears ($\partial v / \partial x < 0$) are shaded. Surface current vectors are shown. Thick dotted lines denote slack water (northward and southward current components are zero).

Occurrences of (H)igh and (L)ow tides indicated on right side of plot. (Bottom) Bottom depth profile along section.

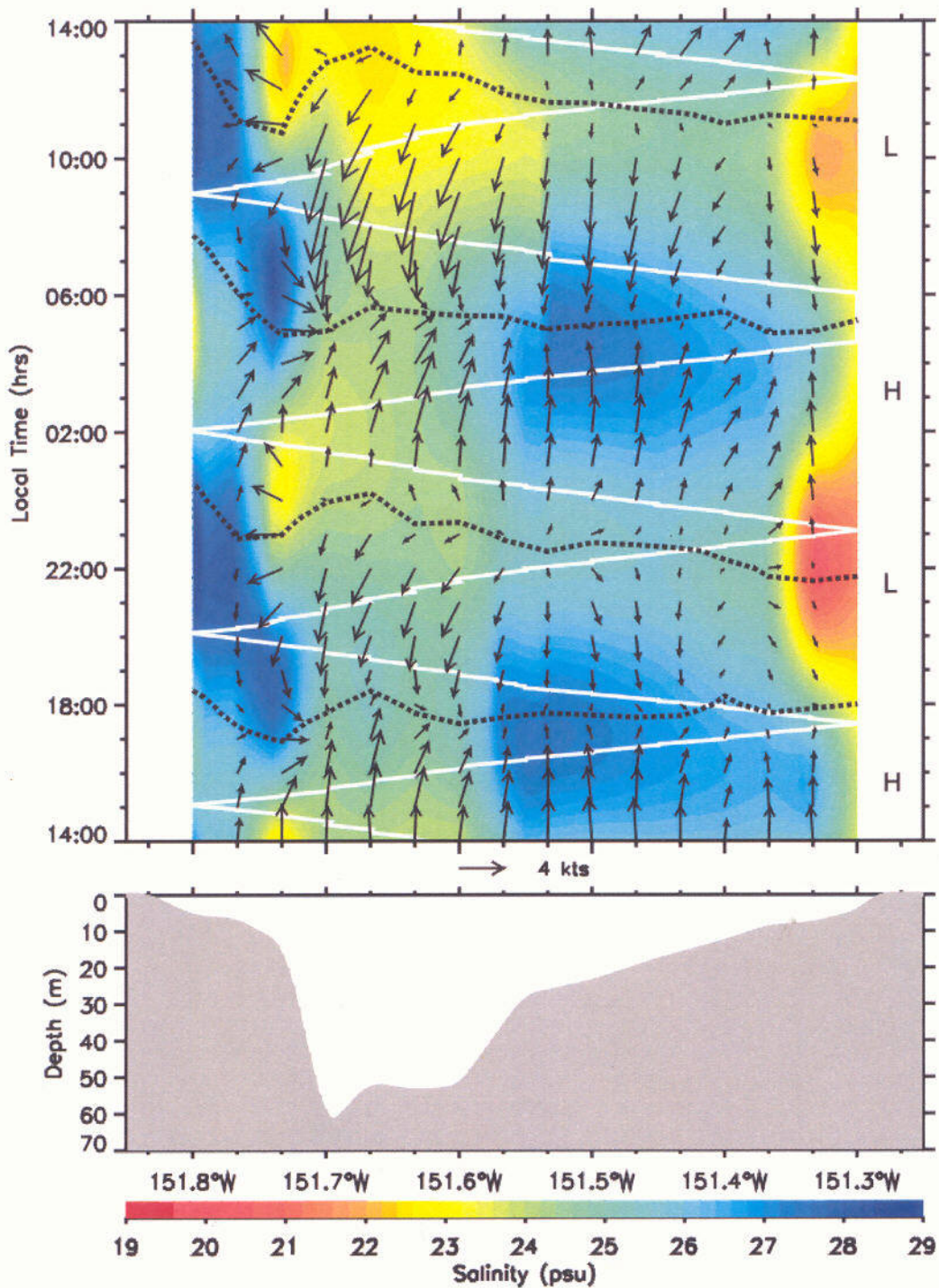


Figure 17. (Top) Time-longitude plot of surface layer salinity (0–1 m). Contour interval is 0.5 psu. Surface current vectors are shown. Thick dotted lines denote slack water (northward and southward current components are zero). Occurrences of (H)igh and (L)ow tides indicated on

right side of plot. White oblique lines indicate vessel position and time. (Bottom) Bottom depth profile along section.



Figure 18. Map of bathymetric gradients in Cook Inlet, Alaska.



Figure 19. Synthetic aperture radar image (8 February 2000) of central Cook Inlet, Alaska.